Journal of Alloys and Compounds 860 (2021) 158257

Contents lists available at ScienceDirect

Journal of Alloys and Compounds

journal homepage: www.elsevier.com/locate/jalcom

Tetragonal to cubic transition of $Sr_{0.8}Dy_{0.2}CoO_{3-\delta}$ and oxygen mobility: TG-DSC-XRD study

Sergei Vereshchagin[a,*], Vyacheslav Dudnikov[b], Yury Orlov[b,c], Leonid Solovyov[a]

[a] Institute of Chemistry and Chemical Technology, Federal Research Center "Krasnoyarsk Scientific Center, Russian Academy of Sciences, Siberian Branch", Krasnoyarsk 660036 Russia
[b] Kirensky Institute of Physics, Federal Research Center "Krasnoyarsk Scientific Center, Russian Academy of Sciences, Siberian Branch", Krasnoyarsk 660036 Russia
[c] Siberian Federal University, Institute of Engineering Physics and Radio Electronics, Krasnoyarsk 660041 Russia

ARTICLE INFO

Article history:
Received 13 December 2019
Received in revised form 1 December 2020
Accepted 6 December 2020
Available online 4 January 2021

Keywords:
Ceramics
Perovskite
Phase transitions
Oxygen mobility
Thermal analysis
X-ray diffraction

ABSTRACT

Processes of ordering (d-o) and disordering (o-d) of Sr^{2+}/Dy^{3+} cations in a single-phase $Sr_{0.8}Dy_{0.2}CoO_{3-\delta}$ was investigated by TG-DSC and XRD as a function of heating/cooling rate (β = 2,10,20,50,99 K min^{-1} and ~50 K/s) in 20% O_2-Ar flow. According to DSC data the interconversion of disordered cubic (*c*) and ordered tetragonal (*t*) structure appears at 1276–1328 K as a first-order phase transition; the temperature and enthalpy of o-d transformation have only slight dependence on β whereas the characteristics of reversed d-o process vary greatly with cooling rate. XRD powder patterns of all samples showed no indications of a simultaneous presence of *c+t* domains, pointing to a single phase composition (*c* or *t*). It was suggested that the observed behavior is a consequence of two simultaneous interconnected processes of A-sublattice melting and cation/ (anion vacancy) ordering. A rarely used novel TG-DSC method based on variable gas phase composition was utilized to study properties of mobile oxygen over $Sr_{0.8}Dy_{0.2}CoO_{3-\delta}$ samples. It was shown that the appearance of tetragonal phase reduces both oxygen mobility and its bonding energy, the latter decreasing substantially only at high degree of Sr^{2+}/Dy^{3+} ordering.

1. Introduction

Mixed oxides $(A'_{1-x}A"_x)B'_{1-y}B"_yO_{3-\delta}$ with perovskite structure ABO_3 make it possible to realize the great diversity of different iso- and heterovalent substitutions. They are ideal systems for fundamental research and attract close attention to yield practically valuable materials (solid oxide fuel cells, catalysts, thermoelectric materials, etc. [1–4]).

It is generally accepted that a key mechanism by which the physical and chemical properties of mixed perovskites can be tuned is through the manipulation of nature of A and B cations and metal oxidations states [5]. Although often both A′ and A" (or B′/B") cations have the same topology in the structure they may adopt different patterns of chemical order [6] ranging from totally disordered system (with random distribution of A′/A" and/or B′/B" over respective crystallographic sites) to the system with ordered arrangement of cations and oxygen vacancies, the latter being thermodynamically stable at temperatures up to 973–1273 K depending on the type of A/B cation [7,8]. Slow cooling from high temperature results in disorder-order phase transition, but disordered phases can exist at T < 900 K as metastable states produced by quenching.

Transitions associated with order–disorder phenomena are found in a wide range of materials and may have a significant impact on their physical and chemical behavior. Recent studies indicate that practically important properties of perovskites can be tuned not only by changing the chemical nature of constituent cations and their arrangements in the structure but also via constructing a proper structured multiphase system. In particular it was shown that the inhomogeneous state of mixed-valence manganites – evidenced by the presence of multiple phase coexistence – is important for the colossal magnetoresistance property [9]. A strategy to decouple thermoelectric parameters for the synergistic optimization of electrical and thermal transport has been developed for high performance thermoelectric materials which take advantage of modulated electronic structure and critical scattering across phase transitions to decouple the power factor and thermal conductivity [10]. Nanoscaled perovskite (La,Sr)$CoO_{3-\delta}$ (LSC) thin-film cathodes exhibit enhanced oxygen surface-exchange properties, if finely dispersed hetero-interfaces of perovskite-like (La,Sr)$2CoO_{4\pm\delta}$ with LSC are

* Corresponding author.
E-mail address: snv@icct.ru (S. Vereshchagin).

https://doi.org/10.1016/j.jallcom.2020.158257
0925-8388/

created at low oxygen partial pressures during a preparation stage [11].

It is known that for $Sr_xLn_{1-x}CoO_{3-\delta}$ systems (*Ln* = Sm-Yb, x = 0.2–0.3) the tetragonal structure with the ordered Sr^{2+} and Ln^{3+} cations and anionic vacancies is thermodynamically stable at ambient temperature [12,13]. Increasing temperature leads to the order-disorder transition but little crystal structural information is available for $Sr_xLn_{1-x}CoO_{3-\delta}$ at high temperatures. The undoped orthorhombic brownmillerite-type $Sr_2Co_2O_{5+\delta}$ itself is known to be stable at T > 1173 K (P_{O2}≈1 Pa) [14]. *Ln*-doping leads to stabilization of cubic (or cubic-like) phases at high temperature as it was shown for $La_{0.6}Sr_{0.4}CoO_{3-\delta}$ [15]; $Gd_{0.2}Sr_{0.8}CoO_{3-\delta}$ [16]; $La_{0.1}Sr_{0.9}Co_{0.9}Fe_{0.1}O_{3-\delta}$, $SrCo_{0.8}Fe_{0.2}O_{3-\delta}$ [17]; $Y_{1/4}Sr_{3/4}CoO_{3-\delta}$ [18].

We have shown recently that A-site Sr^{2+}/Ln^{3+} ordered and disordered $Sr_xLn_{1-x}CoO_{3-\delta}$ (*Ln* = Gd, Dy) phases exhibit completely different performance and that the order-disorder transition has a strong effect on magnetic, transport and catalytic properties [16,19,20]. It was proposed that one can control properties or even create new behavior by changing the ratio of ordered-to-disordered domains and their morphology and therefore it is of prime importance to understand the relationships between the structural and physicochemical characteristics.

Here we describe the preparation of $Sr_{0.8}Dy_{0.2}CoO_{3-\delta}$ samples with ordered and partially/entirely disordered Sr^{2+}/Dy^{3+} arrangement, report their thermochemical behavior revealed by TG-DSC studies, introduce a novel express method of mobile oxygen property testing and disclose the interrelation between the analyzed properties of the samples and the degree of cubic-to-tetragonal structure transformation.

2. Experimental

Sample of $Sr_{0.8}Dy_{0.2}CoO_{3-\delta}$ was prepared by a conventional solid phase ceramic synthesis from Dy_2O_3 (99.99%, metal basis, Alfa Aesar), Co_3O_4 (99.9%, Alfa Aesar) and $SrCO_3$ (99.5%, Reachim) powders. Thoroughly weighted amounts of compounds were ground in an agate mortar with ethanol, pressed into pellets and calcined at 1473 K for 24 h in air with intermediate re-grinding and re-pelleting. The final ceramic pellets were annealed additionally in air for 24 h.

To prepare ordered tetragonal phase of $Sr_{0.8}Dy_{0.2}CoO_{3-\delta}$ ceramic pellets were cooled down from 1473 K with a ramp rate $\beta = 2$ K min^{-1}. Totally disordered cubic phase was produced by quenching pellets from 1473 K to room temperature, estimated value of β at 1300–1000 K was 4200–1800 K min^{-1}. A set of additional samples was prepared by varying β in interval 10–99 K min^{-1}. To ensure the equilibrium oxygen content the pellets were kept in air for 8 h at 773.0 ± 0.1 K. The $Sr_{0.8}Dy_{0.2}CoO_{3-\delta}$ samples thus prepared are denoted as SDC-*n* hereafter, where *n* is the cooling rate, K min^{-1} (Table 1).

Specific surface areas (S) of the samples were found to be 0.07–0.1 m^2 g^{-1} (liquid N_2 single point BET measurements, Nova 3200e Quantachrome Instruments, USA), standard uncertainty of S was 0.05.

X-ray powder diffraction data (XRPD) were collected on a PANalytical X′Pert PRO diffractometer (Appendix A). The full-profile crystal structure analysis was done using the Rietveld method with the derivative difference minimization (DDM) refinement [21].

Oxygen nonstoichiometry δ of SDC-2 and SDC-3000 samples was calculated from the results of the thermogravimetric reduction [22], assuming that the cobalt is reduced to the metallic state. The reduction was performed on a NETZSCH STA 449 C analyzer in a stream of argon with 5% H_2, heating the samples up to 1173 K with a rate of 10 K min^{-1}. The measurements were carried out with correction for the buoyancy force. The process was carried out in Al_2O_3 crucibles with percolated lids, a sample mass of 22 ± 0.5 mg. The standard uncertainty of a non-stoichiometry index $z = 3-\delta$ (calculated from reduction data) was 0.0036. Non-stoichiometry indexes z_i of SDC-10 - SDC-99 was calculated from the mass variation during cooling/heating cycles from 773 to 1473 K under 20% O_2-Ar feed with regard to SDC-2 as $z_i = 2.65 + \Delta\delta_i$, assuming that at T > 1300 K the stoichiometry is independent on thermal history. The standard uncertainty of $\Delta\delta_i$ was 0.05.

STA experiments were performed on a TG-DSC NETZSCH STA 449 C analyzer equipped with an Aeolos QMS 403 C mass spectrometer. The TG-DSC measurements were carried out under dynamic 20%O_2-Ar atmosphere at P = 101 kPa in Pt crucibles with perforated lids. For a run a monolith polycrystalline sample about 1.5×2x1 mm (16–20 mg) was used.

Experiments with variable oxygen partial pressure ("pulse" runs) were conducted using 25 mg of a crushed and sieved sample (0.1–0.2 mm) in open Pt crucibles. The sample was heated up to 773 K (β = 10 K min^{-1}, 20%O_2-Ar) and equilibrated for one hour. After that, the gas flow was switched according to the following time–-chart: 20%O_2/Ar(15 min) – Ar(1 min) - 20%O_2/Ar(15 min) – Ar(1 min) - 20%O_2/Ar(15 min) – Ar(1 min). Initially rectangular O_2 profile broadened owing to TG-DSC -cell volume and resulting output O_2 concentration contour was close to the Gauss function. All the "pulse" runs were carried out with correction for the buoyancy force, i.e. blank experiments (base line) have been performed at the same conditions with empty crucibles.

The sensor sensitivity was calibrated via C_p measurements of the sapphire disk [23] and crosschecked at different cooling rates by measuring Au (Al_2O_3 crucible, NETZSCH standard, T_m = 1335.2 K, ΔH = 63.7 J g^{-1}), standard uncertainty of ΔH measurements was 0.04.

3. Results and discussion

3.1. Structure of ordered and disordered $Sr_{0.8}Dy_{0.2}CoO_{3-\delta}$

The Sr-Dy-Co perovskite annealed from 1473 K (2 K min^{-1}) and equilibrated with oxygen at 773 K (20% O_2-Ar) has composition of $Sr_{0.8}Dy_{0.2}CoO_{2.65}$ (SDC-2, Table 1). The PXRD pattern of the sample is presented in Fig. 1(t-(**I**)). The full-profile structure analysis using the Rietveld method with the DDM refinement has shown that besides the main tetragonal phase minor admixtures of cobalt oxide and

Table 1
Crystallographic parameters and non-stoichiometry of $Sr_{0.8}Dy_{0.2}CoO_{3-\delta}$ samples cooled down from 1473 K with rates of 2–3000 K min^{-1}.

Sample	β, K min^{-1}	3-δ	Symmetry	*a*, nm	*c*, nm
SDC-2, ordered	2	2.65(1)	*I4/mmm*	0.76716(3)	1.5366(1)
SDC-10	10	2.67(1)	*I4/mmm*	0.76671(3)	1.5353(1)
SDC-20	20	2.68(1)	*I4/mmm*	0.76632(4)	1.5344(1)
SDC-50	50	2.70(1)	*I4/mmm*	0.76657(5)	1.5332(1)
SDC-99	99	2.71(1)	*Pm3m*	0.383121(5)	
SDC-3000, disordered	~3000[a]	2.72(1)	*Pm3m*	0.382955(6)	
SDC-3000 –1253 K[b] (see text)	~3000	n.d.	*Pm3m*	0.382921(7)	

n.d. – not determined.
[a] estimated cooling rate at 1250–1350 K.
[b] annealed additionally at 1253 K.

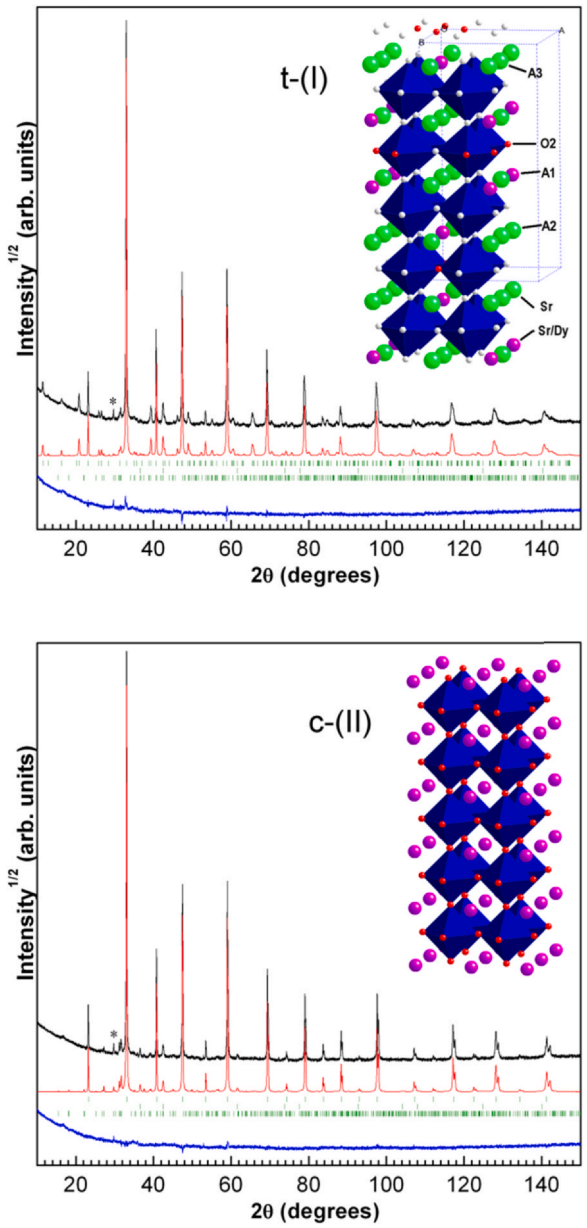

Fig. 1. Observed (top, black), calculated (middle, red), and difference (bottom, blue) X-ray diffraction patterns for ordered (t-(I)) and disordered (c-(II)) samples $Dy_{0.2}Sr_{0.8}CoO_{3-\delta}$ after crystal structure refinement by the DDM method. The calculated peak positions of the main phase and minor admixtures of cobalt oxide and Sr_2SiO_4 are marked by ticks. The Cu K_β line of the main reflection is marked by the asterisk. The insets show structures of ordered tetragonal t-(I) and disordered cubic c-(II) $Sr_{0.8}Dy_{0.2}CoO_{3-\delta}$. Blue octahedra represent Co^{n+}, green spheres represent Sr^{2+}, magenta spheres represent Dy^{3+}/Sr^{2+} and smaller red/gray spheres are oxygen (red color stands for predominant sites of O-vacancy location). Color online.

Sr_2SiO_4 (total estimated amount less than 2 wt%, calculated peak positions are marked by ticks) are present, the latter were formed most probably during the intensive repetitive regrinding in an agate mortar. According to the full-profile structure refinement, the structure of the main phase is identical to that described in [12] and observed earlier by us for $Sr_{0.8}Gd_{0.2}CoO_{3-\delta}$ [16,24]. It corresponds well to the tetragonal *I4/mmm* superstructure t-(**I**) with ordered Dy^{3+}/Sr^{2+} cations and anion vacancies (Fig. 1) and accommodates three distinct crystallographic A-positions for Dy^{3+} or Sr^{2+} ions and four positions for O^{2-}. A2 and A3 sites are occupied exclusively by Sr^{2+} (Fig. 1); shown as green spheres) while A1 site (shown as magenta spheres) may contain both Dy^{3+} and Sr^{2+} ions. The regular alternations of pure Sr^{2+} positions in the ordered state are accompanied, as well, by regularities in the distribution of oxygen vacancies (which are located in O2-sites) and CoO_6 octahedra tilting.

The SDC-3000 sample (quenched from 1473 K, about 50 K s^{-1} at 1250–1350 K, equilibrated with oxygen at 773 K, 20% O_2-Ar) has composition of $Sr_{0.8}Dy_{0.2}CoO_{2.72}$ (Table 1). Similar to SDC-2 the PXRD profile indicates the presence of the same amount of cobalt oxide and Sr_2SiO_4 admixtures, Fig. 1, c-(I). The result of the full-profile structure refinement shows that the structure of the main phase can be described as a cubic perovskite c-(II) with equivalent A-sites which are occupied by either Dy^{3+} or Sr^{2+} in a random order (Fig. 1; magenta spheres). Oxygen vacancies are randomly distributed over the respective O-sites.

3.2. Observation of phase transition of $Sr_{0.8}Dy_{0.2}CoO_{3-\delta}$ by TG-DSC

In general, the behavior of $Sr_{0.8}Dy_{0.2}CoO_{2.65}$ resembled that of $Sr_{0.8}Gd_{0.2}CoO_{2.63}$ described earlier [24]. When heated in 20% O_2-Ar flow $Sr_{0.8}Dy_{0.2}CoO_{2.65}$ started losing oxygen at about 773 K with the gradual mass decrease (reaction 1). A pronounced endo-effect was observed at T_D = 1386 K and it was ascribed (similar to Sr-Gd-Co system) to tetragonal-to-cubic order-disorder (od) transition (reaction 2, Fig. 2a), the position of DSC-effect did not depend on the scanning rate β within experimental error of T_D determination (Fig. 2b). The enthalpy of the transformation was found to be $\Delta H = 40.5 \pm 3.1$ J g^{-1} (β = 2 K min^{-1}).

During cooling from 1473 K (β = 10 K min^{-1}) a distinct exothermic peak (do - disorder-order transition) was observed at T_O = 1309 K

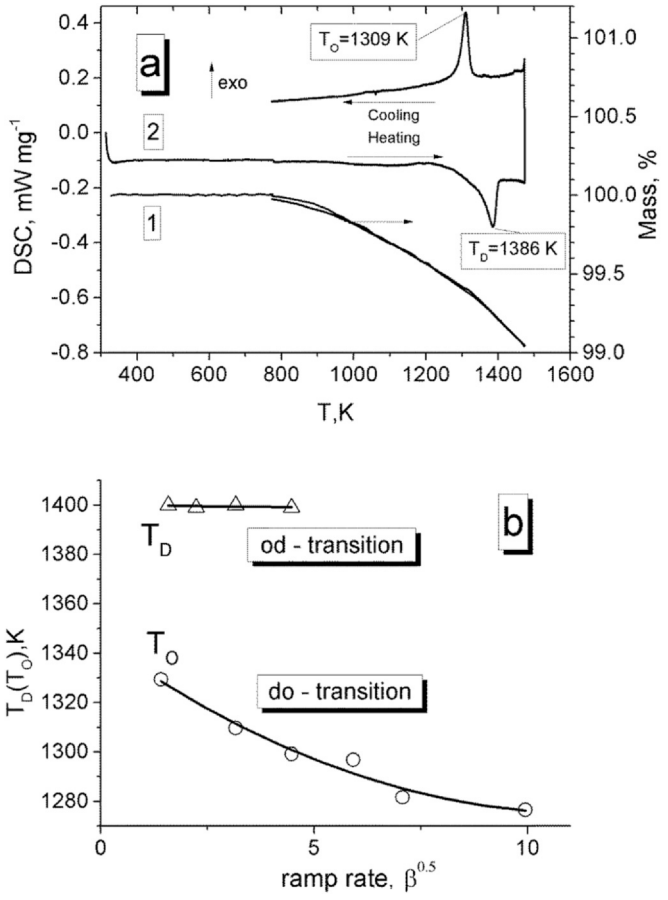

Fig. 2. (a) – TG (1) and DSC (2) signals for heating/cooling cycle (16.0 mg $Sr_{0.8}Dy_{0.2}CoO_{2.65}$; feed 20% O_2-Ar, 50 ml min^{-1}; β = 10 K min^{-1}). T_D and T_O – temperatures of DSC peak extremum for o-d and d-o phase transitions, respectively. (b) – T_D and T_O variation as a function of heating (Δ) or cooling (o) rate.

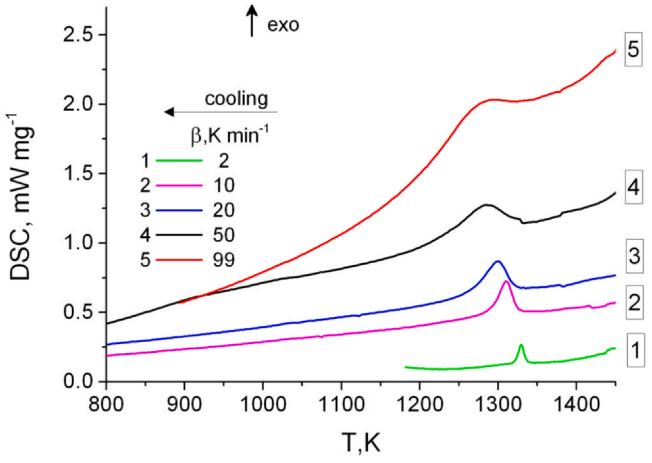

Fig. 3. Variation of DSC cooling profiles (1473–773 K) as a function of ramp rate β, K min^{-1}: 2 (1, green), 10 (2, magenta), 20 (3, blue), 50 (4, black) and 99 (5, red), color online. Sample mass 16–20 mg, feed 20% O_2-Ar, 50 ml min^{-1}.

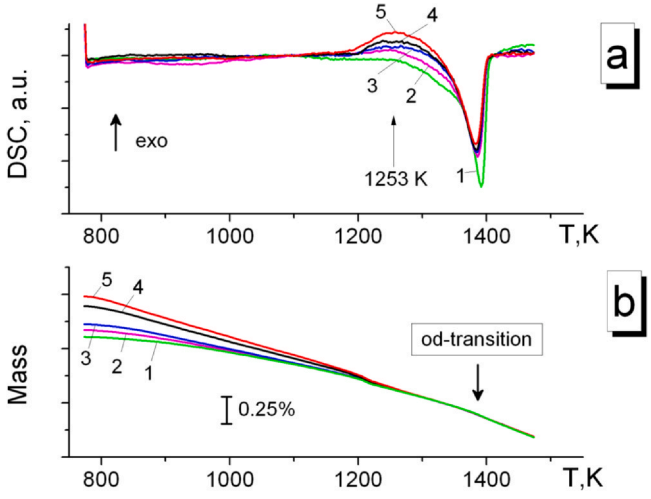

Fig. 4. Variation of DSC (a, curves are overlaid for a comparison) and TG (b) heating profiles (773–1473 K, β = 10 K min^{-1}) for SDC-2 (1, green), SDC-10 (2, magenta), SDC-20 (3, blue), SDC-50 (4, black) and SDC-99 (5, red), color online.

against the background of the progressive mass increase (Fig. 2a) pointing out a reversible character of the transformation. Corresponding TG-curves for heating/cooling cycles almost coincide testifying high oxygen mobility.

$$Sr_{0.8}Dy_{0.2}CoO_{3-\delta 1} = Sr_{0.8}Dy_{0.2}CoO_{3-\delta 2} + (\delta_1-\delta_2)/2\ O_2 \quad (1)$$

$$\text{tetragonal}\text{–}Sr_{0.8}Dy_{0.2}CoO_{3-\delta} = \text{cubic}\text{–}Sr_{0.8}Dy_{0.2}CoO_{3-\delta} \quad (2)$$

Opposite to T_D (heating DSC-curves) the cooling profiles show an evident shift of T_O with a variation of the ramp rate β (Figs. 2b, 3a). A special procedure [25] was employed to eliminate a methodological error of determination of temperature extremum due to the thermal resistance of the sensor-crucible-sample system. A set of heating/cooling cycles was performed at 1173–1473 K using different ramp rates β and the values of T_D / T_O were plotted versus $\beta^{1/2}$. Extrapolation of these trends to $\beta = 0$ yields the true phase transition temperatures not distorted by methodological errors. Fig. 2b shows T_D and T_O recorded at 2–99 K min^{-1} scanning rates as a function $T_{D,O} = f(\beta^{1/2})$. It is evident from the plot that substantial difference $\Delta T = T_D - T_O \approx 60$ K is observed at β = 0 and it is in agreement with the assumption that the transformation is a first order phase transition.

Parallel to the T_O shift a substantial change of enthalpy of do-transformation is observed, the values decrease from − 40.5 ± 3.1 J g^{-1} (β = 2 K min^{-1}) to − 12.3 ± 4.1 J g^{-1} (β = 99 K min^{-1}). So long as slow cooling (SDC-2) results in the formation of the ordered structure t-(**I**) and quenching (SDC-3000) leads to the metastable c-(**II**) phase one can expect that at intermediate ramp rates we find a partial conversion (inverse reaction 2), and, therefore, the reduction of ΔH value may be attributed to incomplete transformation of disordered c-(**I**) to ordered t-(**II**) phase.

To compare the presumably partially ordered samples of $Sr_{0.8}Dy_{0.2}CoO_{3-\delta}$ a special experiment was performed. A monolith ceramic block of SDC-2 was subjected to successive repetitive cycles inside the DSC cell. Each cycle includes isothermal (773 K, 60 min), heating (773–1473 K, β = 10 K min^{-1}) and cooling (1473–773 K, 2–99 K min^{-1}) segments. This procedure leads to the formation of SDC-2 – SDC-99 under controlled conditions and ensures the best reproducibility of base line/DSC profile due to the constant mass and position of the specimen inside the crucible and the crucible on the sensor. The heating segments of the run (10 K min^{-1}, Fig. 4) were used to compare mass changes and thermal effects; TG-data were utilized to calculate the non-stoichiometry of the SDC-10 – SDC-99 (Table 1).

Experiments showed that the temperatures T_D (endo-effect associated with od-transition for SDC-2 – SDC3000) are situated at 1384–1391 K for all SDC-samples (Fig. 4a). Surprisingly the enthalpies of transformation ΔH_D (area of DSC-peak at ≈1300–1450 K) have only a slight dependence upon thermal history. The highest value is found for SDC-2 (40.5 ± 3.1 J g^{-1}), a reduction of ΔH_D by 19% is observed for SDC-10, while the values of ΔH_D for SDC-20, SDC-50 and SDC-99 are almost equal and make up 70% of the highest value.

The samples SDC-2 – SDC-3000 differ in initial non-stoichiometry but display converging trends of mass loss (oxygen release) so that the difference in position of TG-curves becomes negligible at T > 1250 K (Fig. 4b) indicating that at high temperature all SDC-samples have the identical oxygen content. Therefore the concentration of anion vacancies is nearly the same at T_D for all samples and it is not the oxygen non-stoichiometry which causes difference in ΔH_D-values. In the case of SDC-99 the endo-effect at 1384 K also cannot be a result of Sr/Dy randomization because the crystal structure of SDC-99 corresponds to the disordered cubic perovskite (Table 1, Section 3.3) and one can expect disordering of Sr/Dy-cations only for sample which possesses the ordered (or partially ordered) structure.

The nearly equal values of ΔH_D may be explained if we suppose that $Sr_{0.8}Dy_{0.2}CoO_{3-\delta}$ undergoes transformation like the superionic phase transition. It is known that many substances go through transitions in which one species of ion becomes positionally disordered at temperatures below the melting point of the crystal [26]. This phenomenon is called "sublattice melting" and occurs in materials with a variety of crystal structures. The structure of such compounds may be represented as the superposition of a “molten” sublattice of mobile ions and a rigid “core” which conserves the solid up to the melting point. It is typical for superionic conductors (SIC) which undergo temperature generated order–disorder phase transition when some of the ions are excited in interstitial sites (Frenkel defects), where they are distributed over many vacancies.

The transformation of t-(I) to c-(II) requires Sr^{2+}/Dy^{3+} cation relocation which implies enhanced mobility of ion species located over A-sites. The XRD data of quenched SDC-samples show that t-(**I**)-structure disappears at temperatures $T > T_D$ because of thermally induced replacement of Sr^{2+}-ion by Dy^{3+}. Under the same condition Sr^{2+}-Sr^{2+} and Dy^{3+}-Dy^{3+} displacements are also probable but these rearrangements cannot be monitored directly by XRD. Therefore we may assume that the transition at 1300–1450 K can also be treated

as a "melting" of the A-sublattice, the process of "A-site melting" depending upon thermal pretreatment. The endo-effect at 1384 K for SDC-99 corresponds to "melting" of disordered A-sublattice and that at 1391 K for SDC-2 to the ordered one.

The onset of disorder in many SICs is accompanied by a specific heat anomaly and the entropy associated with the anomaly may be comparable with the entropy of melting [26,27]. According to the TG-data the stoichiometry of SDC-2 at 1391 K is $Sr_{0.8}Dy_{0.2}CoO_{2.44}$ therefore the changes of reduced entropy associated with DSC-peak (SDC-2) may be estimated as $\alpha = \Delta S/R = \Delta H/T/R = 40.5 * 200.6/1391/8.31 = 0.70$ (R is the universal gas constant) which is close to the value of the configurational component of the entropy of melting for the cellular model of a liquid $\alpha_m = \ln(2) = 0.693$ [27]. Analogous to the superionic conductors we may suppose that entropy of "melting" of disordered A-sublattice makes the considerable contribution to the total entropy ΔS of the transition [27]. The entropy of "melting" of the ordered sublattice $\Delta S_{ordered}$ is expected to be greater than $\Delta S_{disordered}$ by the value of ΔS_{rand} – configurational component of the entropy (Sr/Dy and O-vacancies randomization) accompanying "melting".

Fig. 4a shows that a special feature of DSC-curve for SDC-2 is a distinct low-temperature shoulder, the intensity of this effect decreasing progressively in the row SDC-2 > SDC-10 > SDC-20~SDC-50~SDC-99. The same effect has been shown recently for $Sr_{0.8}Gd_{0.2}CoO_{3-\delta}$ [24] where changes of anomalous heat capacity in the vicinity of od-transition can be described by superposition of two peaks. Based on the assumption made above one may assign the low-temperature shoulder to the process of Sr/*Ln* (*Ln*=Gd, Dy) randomization while A-sublattice "melting" accounts for the high-temperature part of DSC peak. The reversed picture should be observed in cooling runs – "crystallization" of A-sublattice and ordering of Sr/Ln-cations and oxygen vacancies; it is the latter process, which depends greatly upon quenching rate.

Another peculiarity of DSC-curves for SDC-2 – SDC-3000 is a broad exo-peak located at T > 1175 K which may indicate a slow transformation occurring in the system. No heat evolution is observed for SDC-2 and intensity of the effect increases with growth of the ramp rate β (Fig. 4a). To reveal a possible interrelation between this effect and the ordering/disordering process a special experiment was performed. The fully disordered SDC-3000 (Fig. 4a, curve 5) was annealed at 1253 K (i.e. just before the low temperature shoulder of od-transformation of SDC-2, Fig. 4a, curve 1) and its XRPD pattern was compared with that of the source SDC-3000. No difference was observed, except for a minor decrease of the cell parameter *a* (Table 1) and width of diffraction reflections. It should be pointed out that no superstructural reflections of the tetragonal phase appeared after the annealing which means that the effect may not be associated with the od-transition. Reasonable explanations of the broad exo-effect are equalizing of oxygen content (which is substantially different in SDC-2 – SDC-3000, Table 1) and relieving a stress induced by quenching.

3.3. Observation of $Sr_{0.8}Dy_{0.2}CoO_{3-\delta}$ phase transition by XRD

As follows from Section 3.1, the structure of SDC-3000 corresponds to the cubic perovskite with equivalent A-sites which are occupied by either Dy^{3+} or Sr^{2+} randomly (Fig. 1, c-(II); Fig. 5a, curve 1). The structure of annealed SDC-2 presents the tetragonal *I4/mmm* superstructure with ordered Dy^{3+}/Sr^{2+} cations and anion vacancies (Fig. 1, t-(I); Fig. 5a, curve 5). Intermediate cooling rates ($\beta = 99–10\ K\ min^{-1}$) result in diffraction patterns with progressive high-angle shift of main reflections and gradual rise of intensity of superstructural ones (Fig. 5a, 5b) which become visible at $\beta \le 50\ K\ min^{-1}$.

Thermal behavior of the process under study fits the criteria of the first order phase transition (Section 3.2) which implies the

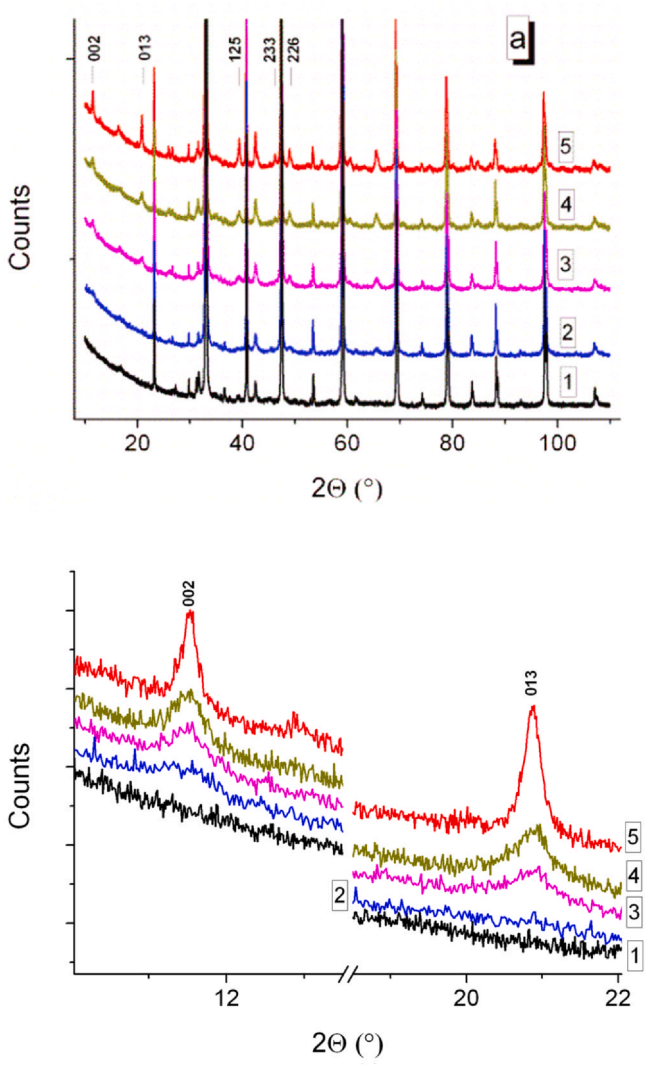

Fig. 5. (a) - XRPD patterns for 1 - SDC-3000 (black), 2 - SDC-50 (blue), 3 - SDC-20 (magenta), 4 – SDC-10(olive), 5 - SDC-2 (red). Some of superstructural reflections of the tetragonal phase are indexed. (b) – enlarged region of [002] and [013] superstructural reflections, color online.

nucleation-growth model for the description of a new phase formation and coexistence of interconvertible phases. That is true, for example, for disordering of perovskite-like brownmillerite-type $Ca_2Fe_2O_5$ compounds [28]. It was shown by in-situ high-temperature single-crystal X-ray diffraction experiments that transformation of low-temperature modification of $Ca_2Fe_2O_5$ with ordered configurations of the tetrahedral chains (space groups *Pnma* or *I2mb*) to a high-temperature statistically disordered form (space group *Imma*) includes a phase coexistence over a range of ca. 25 K. Therefore one can expect that in our case we find a system of the two simultaneously occurring c-(I) and t-(II) phases for the samples cooled down with intermediate rates ($\beta = 99–10\ K\ min^{-1}$). However, XRD data of SDC-10 - SDC-50 specimens show no indications of a combined presence of the c-(I) and t-(II) domains. Instead the XRD patterns reveal a single phase with crystal cell parameters of cubic or tetragonal lattice depending on the thermal history, Table 1.

There is only a limited number of studies devoted to the order-disorder transition in perovskites with detailed analysis of structures of the phases at equilibrium state. Some authors note that identification of a multiphase equilibrium is a challenging task in certain cases. In particular, structural studies using synchrotron X-ray

diffraction, Mössbauer spectroscopy and high-resolution transmission electron microscopy have shown that XRD data failed to detect a multiphase composition of strontium ferrites [29], if the solid is composed of coherently bound nanodomains of perovskite and vacancy-ordered phases. Similarly, it was shown that nanostructured cubic $La_{1-x}Ba_xFe_{0.5}Mn_{0.5}O_3$ (x = 0.25, 0.33 and 0.5) perovskites display the weak superstructure spots in electron diffraction pattern due to cationic ordering in all the samples, though such ordering is not detectable in X-ray diffraction [30]. It was also evidenced [31], that XRPD pattern of nanoscale-structured $LaBaCoO_6$ was very similar to that observed for the completely disordered phase, though it consisted of 90° oriented of 112-type ordered $LaBaCoO_6$ domains detected by transmission electron microscopy.

In our case, a coexistence of domains with ordered and disordered structure is a subject of discussion. At the moment, the experimental data presented above do not enable us to distinguish between two possible models of the solid, namely: (i) coherently bound disordered and ordered nanodomains and (ii) progressive changes of site occupancy from random (c-(II); A1 = A2 = A3 = Sr^{2+}/Dy^{3+}, Fig. 1) to totally ordered (t-(I); A1 = Sr^{2+}/Dy^{3+}, A2 = A3 = Sr^{2+}) according to the second order transition with Dy^{3+} relocation from A2/A3 to A1 site. Additional studies of the materials on the atomic scale using HRTEM are necessary to resolve this ambiguity.

A transformation of c-(II) *Pm3m* structure to the t-(**I**) compound with the tetragonal superstructure *I4/mmm* leads to the increase of the crystal cell dimension in a regular manner ($a_p \times a_p \times a_p \rightarrow 2a_p \times 2a_p \times 4a_p$, a_p – crystal cell parameter of parent perovskite). Therefore, to monitor the progress of the conversion it is convenient to use reduced *a*-parameter, which is equal to a_p for cubic and *a*/2, *c*/4 for tetragonal phase (Fig. 6).

The results show (Fig. 6) that there is a gradual increase of the volume of ABO_3 unit V_{corr} (a^3 for cubic and $a^2c/16$ for tetragonal structure) with decreasing cooling rate β. At $\beta \geq 50\ K\ min^{-1}$ the isotropic expansion of the crystal cell occurred ($a = c/2$) and at $\beta < 50\ K\ min^{-1}$ the anisotropic growth of V_{corr} is observed ($a \ddagger c/2$).

A monotonic increase in values *of a* or *c/4* parameters with decreasing β let us describe completeness of c-(II) to t-(I) transformation using a relative difference in cell dimension (*ε*-value, Eq. 3),

$$\varepsilon = \frac{a - a_{SDC-3000}}{0.25c_{SDC-2} - a_{SDC-3000}} \quad (3)$$

where *a* – reduced crystal cell parameter.

It is interesting that ΔH_O (exo-effect in cooling DSC segment, Fig. 3) is proportional to the *a (or c/4)* parameters (Fig. 6) and it means that either of the two values may be used to characterize the degree of c-(I) to t-(II) transformation.

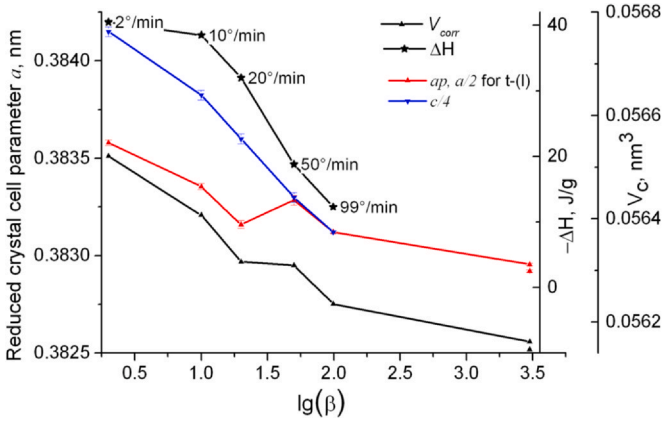

Fig. 6. Variation of reduced crystal cell parameters *a*, V_{corr}, and enthalpy of transition ΔH (cooling segment) as a function of cooling rate β.

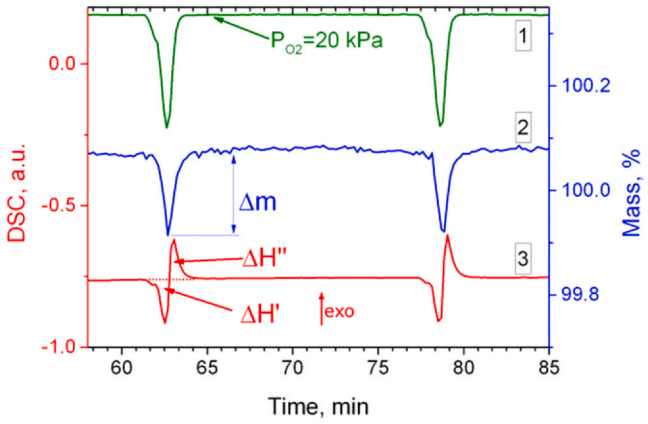

Fig. 7. Typical profiles of mass-spectral intensity of O_2^+ ion *m/z* = 32 (1, olive, color online), TG (2, blue) and DSC-signal (3, red) under stepwise change of O_2 concentration at 773 K for SDC samples (25 mg, crushed and sieved 0.1–0.2 mm). Purging gas: (20%O_2/Ar) – (Ar) – (20%O_2/Ar) - (Ar) – (20%O_2/Ar). Color online.

3.4. Studies of oxygen mobility by TG-DSC under non-stationary gas phase composition

To reveal interrelations between o-d transition and properties of mobile oxygen we apply a STA-based "pulse" procedure developed earlier for Sr-Gd-Co perovskites [32]. When a Gauss-like O_2 concentration contour (Fig. 7, curve 1) was applied to a sample inside DSC cell an evident change of sample mass was observed (Fig. 7, curve 2): a decrease of O_2 partial pressure results in oxygen liberation (Eq. 1) with respective mass reduction and endothermic DSC-effect (Fig. 7, curve 3, ΔH'); an increase of oxygen concentration leads to sample oxidation (O_2 consumption) and restoration of the mass accompanied with exothermic peak (ΔH").

It is necessary to note that the sample mass before and after repetitive cycles remained invariable and the absolute values of ΔH' and ΔH" (estimated from the peak areas) were identical within experimental errors. These observations point to the high reversibility of red-ox process (Eq. 1) and make it possible to estimate the amount of oxygen removed (Δn=Δm(%)/16/100/1000, mg-atom O/g) in a single cycle from Δm value. In this case the ratio $\Delta H_\beta = \Delta H'/\Delta n$ gives an estimation of enthalpy of oxygen removal (at given *δ*).

Calculated in such a way the values of Δn and ΔH_β are shown in Fig. 8 as a function of *ε* (completeness c-(**II**) to t-(**I**) transformation, Eq. 3). The results indicate that ΔH_β has only a slight tendency to go down with *ε* and displays the main change in the region of high ordered structures (*ε* > 0.74). As opposed to the enthalpy a considerable reduction of Δn with *ε* is observed, the amount of oxygen removed/recovered per a single "pulse" corresponding to a few O-monolayers (assuming a monolayer capacity of $2.25 \cdot 10^{-5}$ g-atom O m^{-2}). Therefore it is not surface oxygen which is responsible for observed TG-DSC effects and the values of Δn can be used as a measure of oxygen mobility together with the ΔH_β values which reflect primarily properties of mobile bulk oxygen.

The influence of cation ordering on oxygen diffusivity in Co-containing perovskites has been studied already. It was shown that the improvement of the oxygen transport properties was induced by the cation ordering in half-doped $GdBaM_2O_{5+x}$ perovskites (M=Mn,Co) due to the formation of a disorder-free layered crystal structure [33] and thus suggesting precisely the opposite effect to that we report here for $Sr_{0.8}Dy_{0.2}CoO_{3-\delta}$ and earlier for $Sr_{0.8}Gd_{0.2}CoO_{3-\delta}$ [16,32]. It is not surprising because accelerated molecular dynamics calculation revealed that the nature of oxygen vacancy diffusion may vary with A-cation ordering in double Ti-perovskites from one-dimensional to three-dimensional and the mobility may be both higher and lower than either of the two end

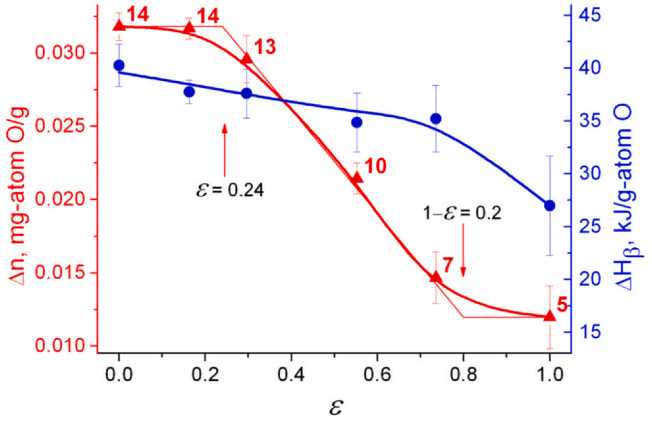

Fig. 8. Variation of amount of oxygen removed/recovered (▲?, per pulse) and enthalpy of its abstraction (● ?) as a function of ε (completeness c-(II) to t-(I) transformation, Eq. 3). Figures near points stand for a formal number of O-monolayers removed/recovered per pulse, whiskers are estimates of standard uncertainties, color online.

member single compounds [34]. The different influence of A-cation ordering on the oxygen mobility can be explained from structural peculiarities of the perovskites. A half-doped $LnBaM_2O_{5+x}$ binary oxides adopt an ordered crystal structure $LnBaMn_2O_6$ with alternating LnO and BaO layers along the c axis (2D layered ordering [6]). Oxygen vacancies reside in lanthanide planes, providing a possibility of a fast 2D diffusion of oxygen. In the case of tetragonal $Sr_{0.8}Ln_{0.2}CoO_{3-\delta}$ the pattern of Sr/Ln ordering is 1D columnar, anion vacancies are localized exclusively at O2-position, which form isolated 4-member clusters (room temperature, Fig. 1) and hampered oxygen atom rearrangement.

Interestingly, that the $\Delta n=f(\varepsilon)$ curve has three distinct segments (Fig. 8): Δn is roughly proportional to the progress of ordering process at $\varepsilon = 0.2–0.74$ but it undergoes only negligible variations at $\varepsilon < 0.18$ and, presumably, at $\varepsilon > 0.8$. If we assume, that a quenching leads to formation of coherently bound domains with different degree of structural order and, accordingly, with different local oxygen (anion vacancy) mobility then the behavior of the effective mobility of a partially ordered medium can be described using percolation theory. In this case the intensification of oxygen transport at $0.18 < \varepsilon < 0.8$ can be explained by a formation of an infinite network (cluster) of ordered/disordered domains which occurs at the percolation threshold $x_c = 0.2–0.3$ depending of the type of site connectivity [35]. Fig. 8 shows that onsets of $\Delta n=f(\varepsilon)$ curve satisfactorily match the above-mentioned interval both from disordered ($\varepsilon = 0.24$) and ordered ($1-\varepsilon = 0.2$) sides. Anyway it should be clear that random properties of the partially ordered perovskites that are fixed in space and the connectivity of domains with similar properties played an important role in creation of effective oxygen mobility. The presented data do not allow us for unequivocal determination of the nature of oxygen mobility changes and additional studies at nano-level scale are necessary but they clearly indicate that the applied TG/DTG/MS methodology with variable composition of gas phase can be successfully employed for characterization of dynamic properties of oxygen anions in the oxygen conducting perovskites.

4. Conclusions

A combined TG-DSC and XRPD study is a very convenient approach to elucidate the details of order-disorder transformation of perovskites. The obtained data clearly show that the high temperature Sr^{2+}/Dy^{3+} redistribution in $Sr_{0.8}Dy_{0.2}CoO_{3-\delta}$ is masked by a first order transition of the A-sublattice melting. The quenching of high temperature cubic $Sr_{0.8}Dy_{0.2}CoO_{3-\delta}$ under controlled conditions with different cooling rates gives formally partially ordered samples which do not display XRD-indications for a coexistence of the cubic and tetragonal phases. The progress of cubic-to-tetragonal structure transformation can be monitored using both crystallographic parameters of the cubic/tetragonal structure and the value of exo-effect in cooling DSC segment. A rarely used TG-DSC-MS method based on variable composition of gas phase has been applied to characterize quantitatively the relative mobility of oxygen as an integral process which includes the oxygen bulk diffusion and the oxygen exchange at the interface between the gas and the solid. It was shown that the quenching under controlled condition allows precisely adjusting the cubic-to-tetragonal transformation of the $Sr_{0.8}Dy_{0.2}CoO_{3-\delta}$ perovskite and, accordingly, to change the mobility of oxygen vacancies in the lattice in a predictable required direction. The results demonstrate the potential of using tailored double perovskite structures to precisely control the behavior of oxygen vacancies in these materials.

CRediT authorship contribution statement

Sergei Vereshchagin: Conceptualization, Methodology. **Vyacheslav Dudnikov**: Project administration, Validation. **Yury Orlov**: Investigation, Data curation. **Leonid Solov'yov**: Software, Formal analysis.

Declaration of Competing Interest

The authors declare that they have no known competing financial interests or personal relationships that could have appeared to influence the work reported in this paper.

Acknowledgments

This work was conducted within the framework of the budget project (Project No. AAAA-A17-117021310222-4) for Institute of Chemistry and Chemical Technology SB RAS using the equipment of Krasnoyarsk Regional Research Equipment Centre of SB RAS and in part was funded by Russian Foundation for Basic Research (projects 19-03-00017), RFBR and BRFBR (project 18-52-00017), Russian Foundation for Basic Research, Government of Krasnoyarsk Territory, Krasnoyarsk Regional Fund of Science (project 18-42-243004).

Appendix A. Supporting information

Supplementary data associated with this article can be found in the online version at doi:10.1016/j.jallcom.2020.158257.

References

[1] C. Moure, O. Pena, Recent advances in perovskites: processing and properties, Prog. Solid State Chem. 43 (2015) 123–148.
[2] J. Sunarso, S.S. Hashim, Na Zhu, Wei Zhou, Perovskite oxides applications in high temperature oxygen separation, solid oxide fuel cell and membrane reactor: a review, Prog. Energ. Combust. 61 (2017) 57–77.
[3] Wangcheng Zhan, Yun Guo, Xueqing Gong, Yanglong Guo, Yanqing Wang, Guanzhong Lu, Current status and perspectives of rare earth catalytic materials and catalysis, Chin. J. Catal. 35 (2014) 1238–1250.
[4] R. Pelosato, G. Cordaro, D. Stucchi, C. Cristiani, G. Dotelli, Cobalt based layered perovskites as cathode material for intermediate temperature Solid Oxide Fuel Cells: a brief review, J. Power Sour. 298 (2015) 46–67.
[5] A. Hossain, S. Roy, K. Sakthipandi, The external and internal influences on the tuning of the properties of perovskites: an overview, Ceram. Int. 45 (2019) 4152–4166.
[6] G. King, P.M. Woodward, Cation ordering in perovskites, J. Mater. Chem. 20 (2010) 5785–5796.
[7] J.S. Anderson, Problems of Nonstoichiometry, North-Holland Pub. Co., Amsterdam, 1970, p. 292.
[8] A.I. Gusev, NonstoichioMetry, Disorder, Short- and Long-range Order in Solid, Fizmatlit,, Moscow, 2007, p. 856.
[9] A. Arulraj, R.E. Dinnebier, S. Carlson, M. Hanfland, S. van Smaalen, Strain effects in perovskite manganites, Prog. Solid State Chem. 35 (2007) 367–377.

[10] Chong Xiao, Zhou Li, Kun Li, Pengcheng Huang, Yi Xie, Decoupling interrelated parameters for designing high performance thermoelectric materials, Acc. Chem. Res. 47 (2014) 1287–1295.
[11] J. Hayd, Yokokawa Harumi, E. Ivers-Tiffee, Hetero-interfaces at nanoscaled (La,Sr)$CoO_{3-\delta}$ thin-film cathodes enhancing oxygen surface-exchange properties, J. Electrochem. Soc. 160 (2013) F351–F359.
[12] M. James, D. Cassidy, D.J. Goossens, R.L. Withers, The phase diagram and tetragonal superstructures of the rare earth cobaltate phases $Ln_{1-x}Sr_xCoO_{3-\delta}$ ($Ln^{=}La^{3+}$, Pr^{3+}, Nd^{3+}, Sm^{3+}, Gd^{3+}, Y^{3+}, Ho^{3+}, Dy^{3+}, Er^{3+}, Tm^{3+} and Yb^{3+}), J. Solid State Chem. 177 (2004) 1886–1895.
[13] S.Ya Istomin, O.A. Drozhzhin, G. Svensson, E.V. Antipov, Synthesis and characterization of $Sr_{1-x}Ln_xCoO_{3-\delta}$, *Ln* = Y, Sm–Tm, 0.1≤ x≤ 0.5, Solid State Sci. 6 (2004) 539–546.
[14] J.-C. Grenier, S. Ghobane, G. Demazeau, M. Pouchard, P. Hagenmuller, Le cobaltite de strontium $Sr_2Co_2O_5$: caracterisation et proprietes magnetiques, Mater. Res. Bull. 14 (1979) 831–839.
[15] M. Yashima, T. Tsuji, Structural investigation of the cubic perovskite-type doped lanthanum cobaltite $La_{0.6}Sr_{0.4}CoO_{3-\delta}$ at 1531 K: possible diffusion path of oxygen ions in an electrode material, J. Appl. Crystallogr. 40 (2007) 1166–1168.
[16] S.N. Vereshchagin, L.A. Solovyov, E.V. Rabchevskii, V.A. Dudnikov, S.G. Ovchinnikov, A.G. Anshits, Methane oxidation over A-site ordered and disordered $Sr_{0.8}Gd_{0.2}CoO_{3-\delta}$ perovskites, Chem. Commun., 50 (2014) 6112–6115.
[17] Qinghua Yin, Y.S. Lin, Beneficial effect of order–disorder phase transition on oxygen sorption properties of perovskite-type oxides, Solid State Ion. 178 (2007) 83–89.
[18] S. Fukushima, T. Sato, D. Akahoshi, H. Kuwahara, Order–disorder effect of A-site and oxygen-vacancy on magnetic and transport properties of $Y_{1/4}Sr_{3/4}CoO_{3-\delta}$, J. Phys. Soc. Jpn. 78 (2009) 064706.
[19] V.A. Dudnikov, Yu.S. Orlov, N.V. Kazak, A.S. Fedorov, L.A. Solov'yov, S.N. Vereshchagin, A.T. Burkov, S.V. Novikov, S. Yu Gavrilkin, S.G. Ovchinnikov, Effect of A-site cation ordering on the thermoelectric properties of the complex cobalt oxides $Gd_{1-x}Sr_xCoO_{3-\delta}$ (x = 0.8 and 0.9), Ceram. Int. 44 (2018) 10299–10305.
[20] V.A. Dudnikov, Yu.S. Orlov, S. Yu Gavrilkin, M.V. Gorev, S.N. Vereshchagin, L.A. Solovyov, N.S. Perov, S.G. Ovchinnikov, Effect of Gd and Sr ordering in A sites of doped $Gd_{0.2}Sr_{0.8}CoO_{3-\delta}$ perovskite on its structural, magnetic, and thermodynamic properties, J. Phys. Chem. C 120 (2016) 13443–13449.
[21] L.A. Solovyov, Full-profile refinement by derivative difference minimization, J. Appl. Cryst. 37 (2004) 743–749.
[22] K. Conder, E. Pomjakushina, A. Soldatov, E. Mitberg, Oxygen content determination in perovskite-type cobaltates, Mater. Res. Bull. 40 (2005) 257–263.
[23] Thermal analysis, differential thermal analysis; principles. DIN 51007:1994-06.
[24] S.N. Vereshchagin, V.A. Dudnikov, N.N. Shishkina, L.A. Solovyov, Phase transformation behavior of $Sr_{0.8}Gd_{0.2}CoO_{3-\delta}$ perovskite in the vicinity of order-disorder transition, Thermochim. Acta 655 (2017) 34–41.
[25] K.-H. Illers, Die ermittlung des schmelzpunktes von kristallinen polymeren mittels wärmeflusskalorimetrie (DSC), Eur. Polym. J. 10 (1974) 911–916.
[26] W. Hayes, Superionic conductors, Contemp. Phys. 19 (1978) 469–486.
[27] M.A. Korzhuev, Entropy of crystallization of materials from a "molten" sublattice of superionic conductors, Phys. Solid State 40 (1998) 204–205.
[28] H. Krüger, V. Kahlenberg, V. Petříček, F. Phillipp, W. Wertl, High-temperature structural phase transition in $Ca_2Fe_2O_5$ studied by in-situ X-ray diffraction and transmission electron microscopy, J. Solid State Chem. 182 (2009) 1515–1523.
[29] U.V. Ancharova, Nanodomain structure of perovskite-like nonstoichiometric strontium ferrites with high oxygen deficiency. PhD thesis, Novosibirsk, 2014 (in Rus.).
[30] U. Dutta, A. Hossaina, P.S. Walke, D. Ghosha, N.E. Mordvinova, O.I. Lebedev, A. Haquea, K. Pal, A. Gayen, A.K. Kundu, Md Motin Seikh, Synthesis, structure and magnetic properties of nanodimensional $La_{1-x}Ba_xFe_{0.5}Mn_{0.5}O_3$ perovskites, J. Alloy. Comp. 777 (2019) 1396–1402.
[31] E.-L. Rautama, Ph Boullay, A.K. Kundu, V. Caignaert, V. Pralong, M. Karppinen, B. Raveau, Cationic ordering and microstructural effects in the ferromagnetic perovskite $La_{0.5}Ba_{0.5}CoO_3$: impact upon magnetotransport properties, Chem. Mater. 20 (2008) 2742–2750.
[32] S. Vereshchagin, V. Dudnikov, L. Solovyov, Study of mobile oxygen in ordered/disordered nonstoichiometric Sr-Gd-cobaltate by synchronous thermal analysis, J. Sib. Fed. Univ. Chem. 3 (2017) 346–357.
[33] A.A. Taskin, A.N. Lavrov, Yoichi Ando. Fast oxygen diffusion in A-site ordered perovskites, Prog. Solid State Ch 35 (2007) 481–490.
[34] B.P. Uberuaga, G. Pilania, Effect of cation ordering on oxygen vacancy diffusion pathways in double perovskites, Chem. Mater. 27 (2015) 5020–5026.
[35] B.I. Shklovskii, A.L. Éfros, Percolation theory and conductivity of strongly inhomogeneous media, Sov. Phys. Usp. 18 (1975) 845–862.